

Study of Structural, Electrical, and Dielectric Properties of Hexaferrite-PANI Nanocomposites

Muhammad Ajmal, AM Rana, M. Nauman Usmani

Department of Physics, Bahauddin Zakariya University, Multan, Pakistan

Abstract: Y-type hexaferrite with nominal composition $\text{SrCa}_{0.5}\text{Ba}_{0.5}\text{ZnNiGa}_{0.4}\text{Fe}_{11.6}\text{O}_{22}$ was prepared by sol-gel technique. Conducting polymer, polyaniline was synthesized by chemical polymerization method, and Ferrite-Polyaniline composites with 20 % ferrite (C1), 30% ferrite (C2), and 40% (C3) ferrite were prepared by mechanical blending. The synthesized samples were characterized by XRD, electrical resistivity, and dielectric measurements. At room temperature, the dc resistivity of pure PANI is very low but the resistivity of nanocomposites C1, C2, and C3 increases due to random distribution of ferrite filler particles. The crystallite size was obtained using the Scherrer formula $\sim 21.23\text{nm}$. The permittivity of ferrite-PANI composites is high at lower frequencies due to effective grain boundary contribution and it decreases with the increase in frequency due to conducting grains following the Maxwell Wagner model. The variation in the imaginary part of the dielectric constant and loss tangent with frequency also showed similar behavior. The increase in resistivity and decrease in dielectric constant as a function of composition in nanocomposites make them potential candidates for recording media and chip inductors.

Keywords: Ferrite, Ferrite PANI Nano-composites, Dielectric.

Email: majmal@bzu.edu.pk

1. Introduction

Hundreds of years back the civilizations were named according to the materials used in that era i.e. Stone Age, Bronze Age, and Iron Age. The current era and next age is the age of nanotechnology. The new technology will require materials with enhanced physical and chemical properties. The structure-property correlation has become very crucial for nanotechnology. The unique nanomaterials were first recognized by P. Feynman in his classical lecture titled "There's Plenty of Room at the Bottom" on December 29th, 1959, at the annual meeting of the American Physical Society [2]. It is now well established that there are two ways for the preparation of nanomaterials: bottom-up approach and top-down approach. Mostly the bottom-up approach is used and is more suitable for the synthesis of nanomaterials.

The main focus of Nanotechnology is to achieve the twin goals of determining and considering the properties of matter in a controlled manner at the Nanoscale [1-5]. The small size of particles has a large surface-to-volume ratio that affects the material's properties. Nanoscience plays a

vital role in different branches of science like: chemistry, material science, engineering, physics, telecommunication, computer science, and biomedical sciences [6-7]. In the present study, Y-type hexagonal ferrite with composition $\text{SrCa}_{0.5}\text{Ba}_{0.5}\text{ZnNiGa}_{0.4}\text{Fe}_{11.6}\text{O}_{22}$ with the addition of 20 % ferrite (C1), 30% ferrite (C2) and 40% ferrite (C3) in PANI matrix were prepared to optimize the electrical and dielectric properties for multilayer chip inductors.

2. Experimental Technique

2.1 Synthesis of Ferrite

The samples of Y-type hexaferrite/PANI nanocomposites were synthesized by using the sol-gel auto-combustion method. The starting materials used were $\text{Sr}(\text{NO}_3)_2$, $\text{Ca}(\text{NO}_3)_2$, $\text{Ba}(\text{NO}_3)_2$, $\text{Fe}(\text{NO}_3)_2$, $\text{Ni}(\text{NO}_3)_2$, $\text{Zn}(\text{NO}_3)_2$ and $\text{Ga}(\text{NO}_3)_2$. Citric acid was used as a chelating agent. According to stoichiometric calculations, the required amount of compounds was used to prepare solutions in 100 ml deionized water to make the stock solutions. Afterward, all the stock solutions were mixed in a 500ml beaker at 80°C placed on a hot plate magnetic stirrer. To maintain the pH value of the solution up to 7-8 ammonia solution was added dropwise. Continuous stirring and heating at 80°C caused the evaporation of deionized water and the color of the solution converted into golden yellow and at the end, the black thick gel was formed. When the temperature was increased up to 250°C the burning of gel occurred and gel was converted into ash.

The ash was dried and ground using agate mortar and pestle for 30 min to obtain fine powder. The powder was then sintered at 1000°C for 6 h in tube furnace to obtain the Y- type hexagonal ferrites.

2.2 Synthesis of PANI

Polymer PANI is synthesized using aniline monomer and ammonium persulfate. The calculated amount of aniline and ammonium persulfate (APS) is dissolved in HCl and deionized water and stirred for 20 min. Ferrite particles were dispersed in water in a beaker by sonication for 30 min for homogeneous mixing. These three solutions were uniformly mixed on a stirrer for 1 hour and the pH of the solution was maintained at around 2. The final solution was placed in an ice bath because the polymerization was sensitive to heat. The temperature of the ice bath is kept at 10°C for the polymerization process to initiate and kept for the next 24 hours [2]. After 24 hours the matter was filtered using filter paper and rotatory pump. The pH was maintained at ~ 7 by adding

water repeatedly. When the pH was attained the matter was heated at 80°C in the oven for the next 24 hours and then pelleting it for characterization.

The nanocomposites were prepared by mechanical milling of Y-type ferrite and PANI-polymer.

2.3 X-ray Diffraction

The basic principle of X-ray diffraction is the Bragg law [8];

$$2d\sin\theta = n\lambda \quad (1)$$

Where d is the interplanar spacing, θ is the Bragg angle ‘n =1’ is the order of diffraction and λ is the wavelength of the X-ray source.

In the present study, a Philips PW1710 Diffractometer with a Cu $K\alpha$ radiation source ($\lambda=1.54056$ Å) was used as shown in Fig.1 The phase purity of the sample is measured by comparing the measured 2θ angles (or d-spacing), and intensity of the diffraction peaks with the standard patterns found in the JCPDS card. From XRD measurements the grain size and the lattice parameters (a & c) can be calculated based on the Miller indices of each set of crystal planes [1].

The lattice parameters (a & c) of unit cell volume can be calculated as;

$$\sin^2\theta = \lambda^2/3a^2 (h^2+hk+k^2) + (\lambda^2/4c^2) l^2 \quad (2)$$

$$V = 0.8666 a^2c \quad (3)$$

The lattice parameters (a & c) of the unit cell can also be calculated using the following relation;

$$1 / d_{hkl} = 4 (h^2+ hk + k^2) + l^2 / C^2 \quad (4)$$

Where d_{hkl} is the interplanar spacing and hkl is Miller indices.

The grain size can be calculated using the Scherer formula;

$$D = k\lambda/\beta \cos\theta_B \quad (5)$$

Where $k = 0.89$ is shape constant, β is line broadening at half width of maximum intensity, and θ_B is the Bragg angle.

3. Results and Discussion

3.1 X-ray Diffraction

Fig.1 shows XRD patterns of hexagonal ferrite, $SrCa_{0.5}Ba_{0.5}ZnNiGa_{0.4}Fe_{11.6}O_{22}$, polyaniline (PANI), and their composites. The observed reflections in X-ray diffraction patterns were

compared with JCPDs card No. 00-019-019-0100 and it revealed that the phase precipitated out is Y-type hexaferrite with space group R-3m. It was observed that a couple of peaks were unidentified indicating few traces of impurity peaks. Table I lists the experimental and calculated d-values with corresponding holes. The lattice constants were calculated using eq. 2 for two different peaks with different hicks and it was found that $a = 5.89 \text{ \AA}$ and $c = 43.46 \text{ \AA}$. The diffraction peaks of C1, C2, and C3 shifted minutely toward the lower angles may be due to an increase in the d-values. The structure of polyaniline is amorphous but the addition of ferrite filler in different ratios in polyaniline indicates the co-existence of ferrite-PANI phases [7]. The crystallite size for ferrite was calculated using Scherrer formula $\sim 21.23 \text{ nm}$ [8]. The XRD Pattern of composites C1, C2, and C3 shows that a few peaks have diminished intensity and few are suppressed. This may be due to the polymer (amorphous) matrix, since the ferrite particles are randomly distributed in PANI matrix which is why the intensity fluctuates.

3.2 Room Temperature Resistivity

Fig.2 shows the room temperature resistivity of Polyaniline (PANI), Composites (C1- 20%, C2- 30%, C3-40%), and pure Ferrite (F). It is clear from Fig.2 that the resistivity of pure PANI is less as compared to the composites. When the composite was loaded with ferrite filler the resistivity increased due to the insulating nature of the ferrite and random distribution of ferrite particles in the PANI matrix. It was found that the resistivity of C3 (40%) was high as compared to the resistivity of C2 (30%) and C1 (20%) respectively due to the reason that there is no chemical bonding between the PANI matrix and ferrite filler rather the ferrite particles that have been dispersed randomly in the PANI matrix in the form of an isolated island. Hence the hopping process between Fe^{+3} and Fe^{+2} is restricted thereby resistivity increases [9-11].

4. Dielectric Properties

4.1 Dielectric Constant

Fig.3 depicts the real part of the electrical permittivity of ferrite and its composites (C1, C2, and C3) versus frequency. The dielectric constant (ϵ') was measured by using the formula;

$$\epsilon' = C Ah / \epsilon_0 \quad (6)$$

Where C is the capacitance, A is the surface area of the sample, ϵ_0 is the permittivity of free space and h is the thickness of the sample. It was clear from the graph that the dielectric constant decreases with the increase in frequency. The behavior of frequency dependence of dielectric

constant can be explained concerning types of polarization [6]. It was found that in ferrites there exists a similar behavior between the process of polarization and the conduction process as in metals [12-14]. At low frequencies, the high value of permittivity of ferrite was attributed to space charge polarization and electronic polarization. Electronic polarization also occurs due to ion exchange between Fe^{+2} and Fe^{+3} . Interfacial polarization occurs due to the random distribution of oxygen ions at grain and grain boundaries during the sintering of the sample. Referring to Koops's theory, at low frequencies the grain boundaries contribute to the conduction process, and by that the dielectric constant is high. At high frequencies the conducting grains are effective and the dielectric constant decreases and becomes frequency-independent, the dipoles do not respond to the applied frequency [11, 15].

4.2 Complex dielectric constant (Dielectric loss)

The degradation of energy in dielectric materials can be measured by a complex part of the dielectric constant. Fig.4 represents the plot of dielectric loss versus frequency of ferrite, Polyaniline, C1, C2, and C3 nanocomposites. The results showed that the complex dielectric constant decreases with the increase in frequency [9]. According to Maxwell Maxwell-Wagner's model, the structure of ferrites consists of two layers; that is conducting grains separated by poorly conducting grain boundaries [10, 17]. The complex dielectric constant reveals the energy loss in the sample thereby heat is dissipated within the sample [16-18].

4.3 Tangent Loss

Tangent loss is measured by the following formula:

$$\text{Tan}\delta = \epsilon''/\epsilon' \quad (7)$$

Fig.5 shows the variation of tangent loss Vs frequency. The behavior is analogous to complex dielectric constant but it reveals the phase difference between the current and voltage in the samples. The tangent loss increases with the increase of ferrite filler due to the random distribution of the ferrite particles in the PANI matrix. The decrease in tangent loss with increasing frequency is ascribed to the fact that the hopping frequency of charges cannot follow the external frequency. The value of tangent loss depends on the composition and sintering of the samples [18-21].

4.4 AC Conductivity

Variations of AC conductivity as a function of frequency for the synthesized ferrite polymer composite samples are depicted in Fig. 6. It is obvious from the figure that AC conductivity

increases with frequency. The response of AC-conductivity for all the samples can be explained by the well-known Maxwell-Wagner model [22-25]. Conductivity is low at low frequency due to the effectiveness of highly resistive-grains boundaries. On the other hand, the increase in conductivity with an increase in frequency is due to the contribution of the conducting grains at high frequency and enhancement of the hopping mechanism. AC-Conductivity follows Jonscher's Power law which is given by the relation [26]:

$$\sigma_{ac} = \sigma_{DC} + A\omega^n \quad (8)$$

Where A is the constant, n is the exponential factor and σ_{DC} is the frequency-independent conductivity. Fig. (7) Shows the plot of $\ln\sigma_{ac}$ vs $\ln\omega$ following equation 8. The value of exponent 'n' obtained from the slope of equation 8 comes out to be equal to unity, which is indicative of the hopping conduction mechanism in these samples.

5. Conclusions

In this work, Polyaniline was prepared by chemical polymerization technique and Y-type hexagonal ferrite with composition $\text{SrCa}_{0.5}\text{Ba}_{0.5}\text{ZnNiGa}_{0.4}\text{Fe}_{11.6}\text{O}_{22}$ by sol-gel method. The Ferrites/ PANI nanocomposites such as 20 % ferrite (C1), 30% ferrite (C2), and 40% ferrite (C3) were prepared by mechanical blending. The difference in the real and imaginary part of permittivity in ferrite-PANI nanocomposites showed similar behavior as already reported results. The permittivity of ferrite-PANI composites is high at lower frequencies due to effective grain boundaries and it decreases as the frequency increases due to conducting grains following the Maxwell Wegner model. The change in dielectric loss and tangent loss versus frequency also showed the same trend. At room temperature, the resistivity of pure PANI is low but in the case of composites (C1, C2, and C3) the resistivity increases due to random distribution of filler particles. These low-resistive nanocomposite samples with high permittivity could be the best potential option for multilayer chip inductors.

Table-I XRD analysis: $2\theta^\circ$ values, d-exp, d-calc and helps for $\text{SrCa}_{0.5}\text{Ba}_{0.5}\text{ZnNiGa}_{0.4}\text{Fe}_{11.6}\text{O}_{22}$ Y-type hexagonal Ferrite

Sr. No	$2\theta(\text{degree})$	d-exp. (Å)	d-calc. (Å)	hkl
1	19.273	4.60	4.59	(104)
2	22.601	3.93	3.93	(107)
3	23.979	3.71	3.68	(01 8)
4	24.551	3.62	3.62	(00 12)
5	30.427	2.93	2.92	(110)

6	31.233	2.86	2.86	(113)
7	32.143	2.78	2.79	(1013)
8	33.001	2.71	2.71	(116)
9	33.911	2.64	2.65	(11 14)
10	35.913	2.50	2.5	(119)
11	37.005	2.43	2.43	(2050)
12	37.577	2.39	2.39	(10 16)
13	37.357	2.40	2.35	(02 7)
14	41.269	2.18	2.19	(210)
15	45.403	1.99	2.09	(01 20)
16	49.147	1.85	1.85	(02 16)
17	50.655	1.80	1.8	(20 17)
18	54.217	1.69	1.69	(11 21)
19	55.257	1.66	1.65	(20 20)
20	56.375	1.63	1.63	(1214)
21	57.779	1.59	1.59	(01 26)
22	59.261	1.56	1.56	(02 22)
23	61.185	1.51	1.52	(20 23)
24	63.447	1.46	1.47	(2119)
25	65.069	1.43	1.44	(129)
26	66.957	1.40	1.393	(315)

List of Figures

Fig. 1 X-ray diffraction patterns of $\text{SrCa}_{0.5}\text{Ba}_{0.5}\text{ZnNiGa}_{0.4}\text{Fe}_{11.6}\text{O}_{22}$, C1, C2, C3 and PANI (* indicates rhombohedral Paeks compared with JCPDs card No. 00-019-0100)

Fig. 2 Room temperature Resistivity of $\text{SrCa}_{0.5}\text{Ba}_{0.5}\text{ZnNiGa}_{0.4}\text{Fe}_{11.6}\text{O}_{22}$, C1, C2, C3 and PANI

Fig. 3 Variation of dielectric constant (ϵ') Vs applied field frequency of $\text{SrCa}_{0.5}\text{Ba}_{0.5}\text{ZnNiGa}_{0.4}\text{Fe}_{11.6}\text{O}_{22}$, C1, C2, C3, and PANI.

Fig. 4 Variation of dielectric loss factor (ϵ'') Vs applied field frequency of $\text{SrCa}_{0.5}\text{Ba}_{0.5}\text{ZnNiGa}_{0.4}\text{Fe}_{11.6}\text{O}_{22}$, C1, C2, C3, and PANI.

Fig. 5 Variation of dielectric tangent loss ($\tan \delta$) Vs applied field frequency of $\text{SrCa}_{0.5}\text{Ba}_{0.5}\text{ZnNiGa}_{0.4}\text{Fe}_{11.6}\text{O}_{22}$, C1, C2, C3, and PANI.

Fig. 6 Variation of ac electrical conductivity (σ_{ac}) Vs applied frequency of $\text{SrCa}_{0.5}\text{Ba}_{0.5}\text{ZnNiGa}_{0.4}\text{Fe}_{11.6}\text{O}_{22}$, C1, C2, C3, and PANI.

Fig. 7 Variation of ac $\ln(\sigma_{ac})$ Vs $\ln\omega$ of $\text{SrCa}_{0.5}\text{Ba}_{0.5}\text{ZnNiGa}_{0.4}\text{Fe}_{11.6}\text{O}_{22}$, C1, C2, C3 and PANI.

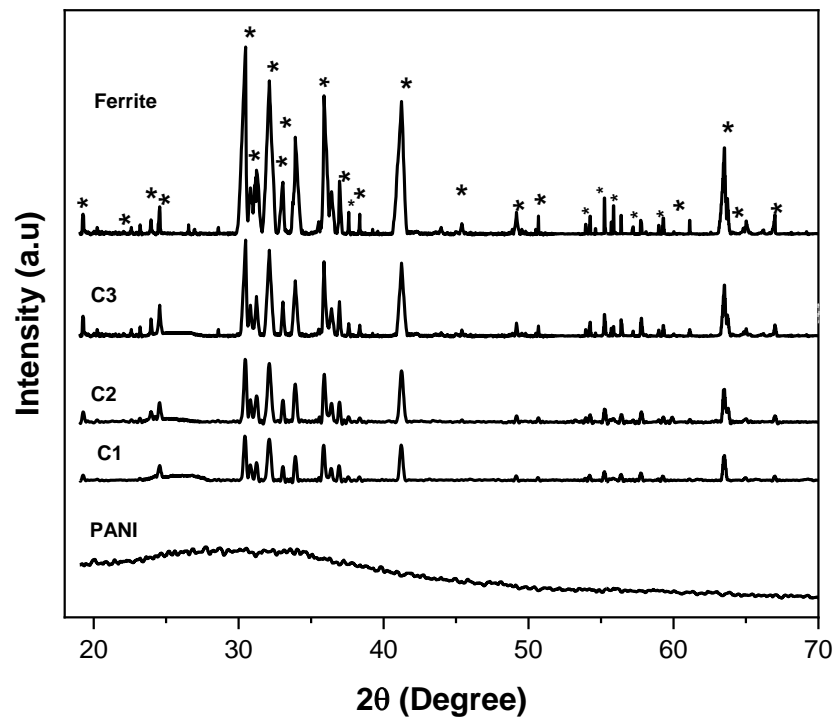
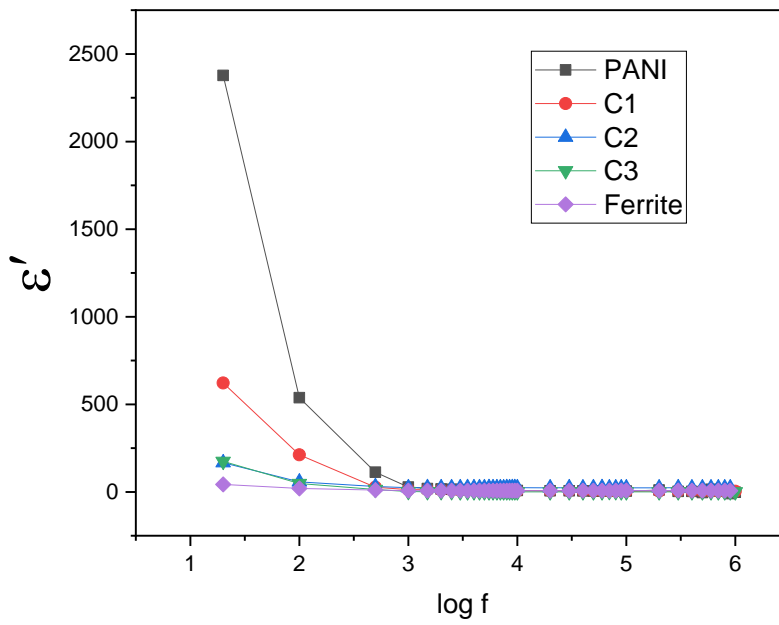
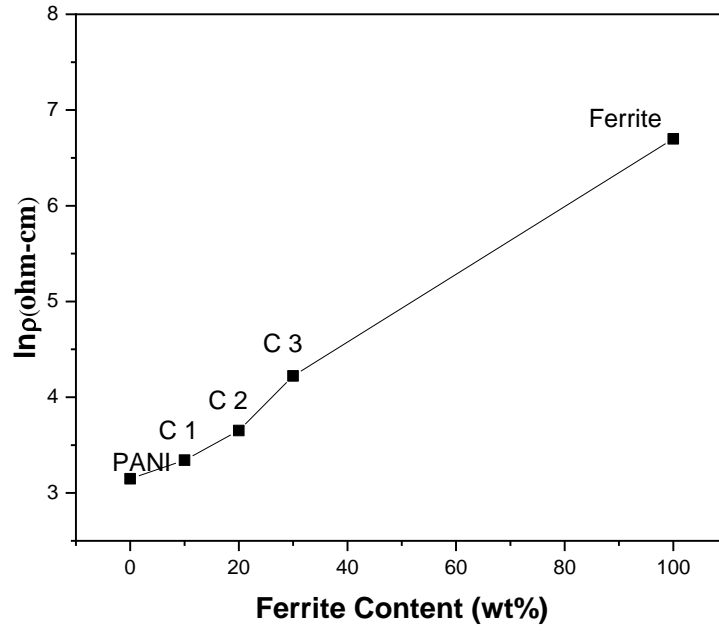
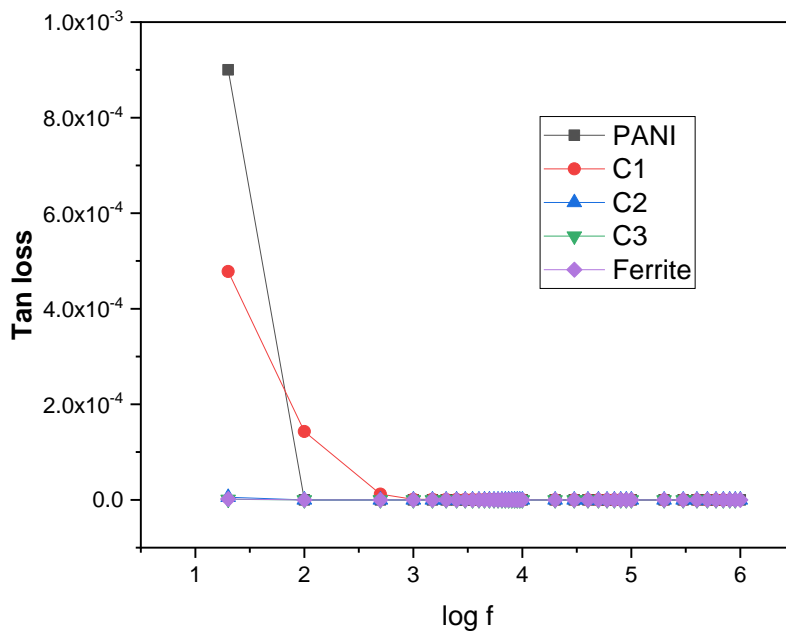
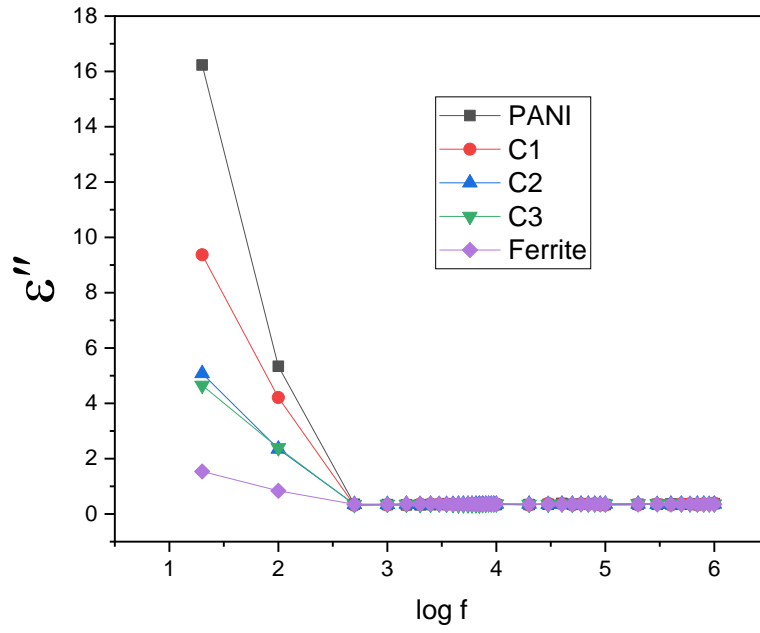
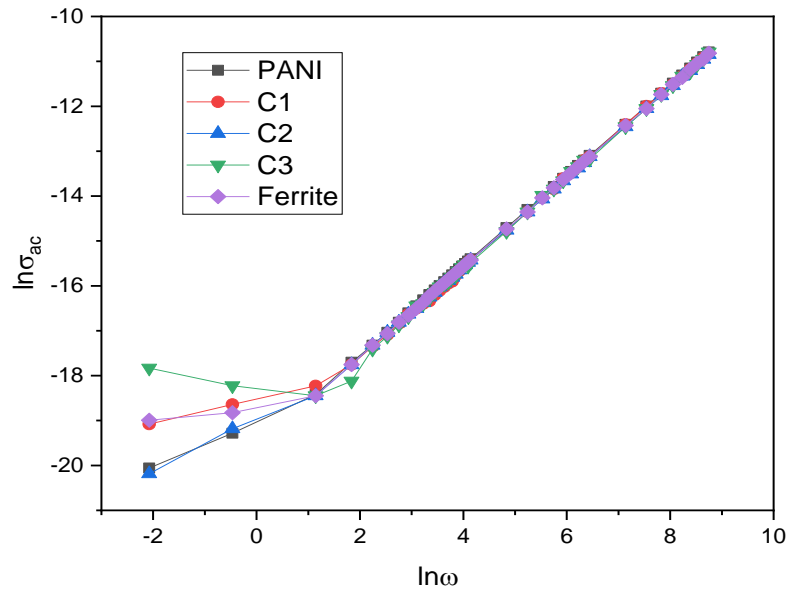
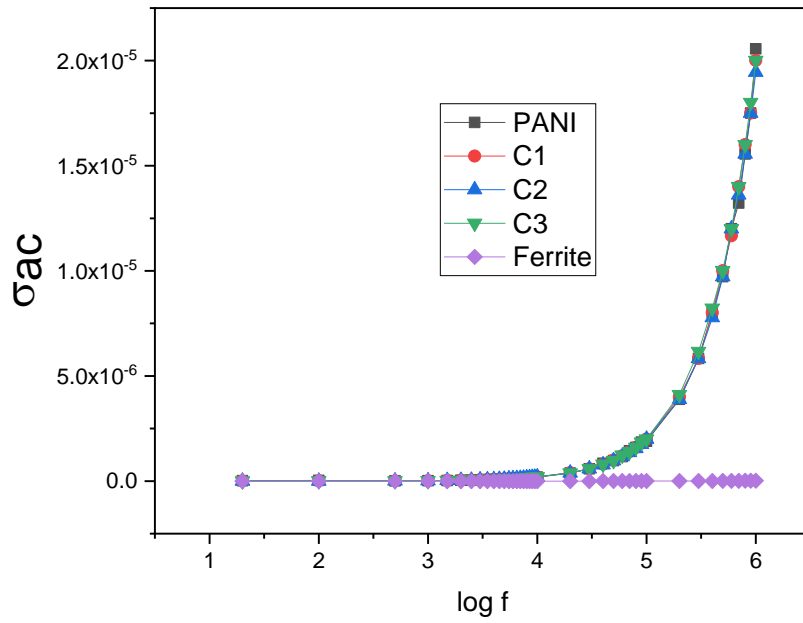


Fig. 1 X-ray diffraction patterns of $\text{SrCa}_{0.5}\text{Ba}_{0.5}\text{ZnNiGa}_{0.4}\text{Fe}_{11.6}\text{O}_{22}$, C1, C2, C3 and PANI (* indicates rhombohedral Paeks compared with JCPDs card No. 00-019-0100)







References

- [1]. Richard P. Feynman, Caltech Engineering and Science, 23(5), Feb. 1960, pp22-36.
- [2]. Lijuan Zhang and Meixiang Wan, "Polyaniline/TiO₂ composite nanotubes," The Journal of Physical Chemistry B **107** (28), 6748-6753 (2003).

- [3]. N Gospodinova and L Terlemezyan, "Conducting polymers prepared by oxidative polymerization: polyaniline," *Progress in Polymer Science* **23** (8), 1443-1484 (1998).
- [4]. V Erokhin, MK Ram, and Ö Yavuz, "The Nanotechnology", Elsevier, London, (2008).
- [5]. A Radhe Shyam, Reena Dwivedi, VS Reddy, KVR Chary, and R Prasad, "Vapour phase methylation of pyridine with methanol over the $Zn_{1-x}Mn_xFe_2O_4$ ($x= 0, 0.25, 0.50, 0.75$ and 1) ferrite system," *Green Chemistry* **4** (6), 558-561 (2002).
- [6]. Vanga S Reddy, A Radhe Shyam, R Dwivedi, RK Gupta, VR Chumbale, and R Prasad, "Ortho-selective vapor phase methylation of phenol over nanocrystalline ferros spinels of varying Zn^{2+}/Mn^{2+} ionic composition," *Journal of Chemical Technology and Biotechnology* **79** (10), 1057-1064 (2004).
- [7]. Yoshiyuki Naito and Kunihiro Suetake, "Application of ferrite to electromagnetic wave absorber and its characteristics," *IEEE Transactions on Microwave Theory and Techniques* **19** (1), 65-72 (1971).
- [8]. HK Chaudhari and DS Kelkar, "X-ray diffraction study of doped polyaniline," *Journal of Applied Polymer Science* **62** (1), 15-18 (1996).
- [9]. JY Shin and JH Oh, "The microwave absorbing phenomena of ferrite microwave absorbers," *IEEE Transactions on Magnetics* **29** (6), 3437-3439 (1993).
- [10]. SS Kim, SB Jo, KI Gueon, KK Choi, JM Kim, and KS Churn, "Complex permeability and permittivity and microwave absorption of a ferrite-rubber composite at X-band frequencies," *IEEE Transactions on Magnetics* **27** (6), 5462-5464 (1991).
- [11]. Andrey N Lagarkov and Konstantin N Rozanov, "High-frequency behavior of magnetic composites," *Journal of Magnetism and Magnetic Materials* **321** (14), 2082-2092 (2009).
- [12]. Mukhtar Ahmad, Qasim Ali, Ihsan Ali, Ishtiaq Ahmad, M Azhar Khan, Majid Niaz Akhtar, G Murtaza, and MU Rana, "Effects of Sr-substitution on the structural and magnetic behavior of Ba-based Y-type hexagonal ferrites," *Journal of Alloys and Compounds* **580**, 23-28 (2013).
- [13]. Attia Aslam, MU Islam, Irshad Ali, MS Awan, Muhammad Irfan, and Aisha Iftikhar, "High-frequency electrical transport properties of $CoFe_2O_4$ and $Sr_2NiMnFe_{12}O_{22}$ composite ferrites," *Ceramics International* **40** (1), 155-162 (2014).
- [14]. Irshad Ali, Abdul Shakoor, MU Islam, Muhammad Saeed, Muhammad Naeem Ashiq, and MS Awan, "Synthesis and characterization of hexagonal ferrite $Co_2Sr_2Fe_{12}O_{22}$ with doped polypyrrole composites," *Current Applied Physics* **13** (6), 1090-1095 (2013).
- [15]. Muhammad Javed Iqbal and Saima Farooq, "Extraordinary role of Ce–Ni elements on the electrical and magnetic properties of Sr–Ba M-type hexaferrites," *Materials Research Bulletin* **44** (11), 2050-2055 (2009).
- [16]. Asmat Elahi, Mukhtar Ahmad, Ihsan Ali, and MU Rana, "Preparation and properties of sol-gel synthesized Mg-substituted Ni_2Y hexagonal ferrites," *Ceramics International* **39** (2), 983-990 (2013).
- [17]. Muhammad Ajmal, M.U Islam, Ghulam Abbas Ashraf, Muhammad Aamir Nazir, and MI Ghouri, "The influence of Ga doping on structural magnetic and dielectric properties of

- NiCr_{0.2}Fe_{1.8}O₄ spinel ferrite," *Physica B: Condensed Matter* (2017). <https://doi.org/10.1016/i.phyb.2017.05.044>
- [18]. Muhammad Ajmal and MU Islam, "Structural, optical and dielectric properties of polyaniline-Ni_{0.5}Zn_{0.5}Fe₂O₄ nano-composites," *Physica B: Condensed Matter* **521**, 355–360 (2017).
- [19]. Muhammad Javed Iqbal and Rafaqat Ali Khan, "Enhancement of electrical and dielectric properties of Cr doped BaZn₂ W-type hexaferrite for potential applications in high-frequency devices," *Journal of Alloys and Compounds* **478** (1), 847-852 (2009).
- [20]. Takanori Tsutaoka, "Frequency dispersion of complex permeability in Mn–Zn and Ni–Zn spinel ferrites and their composite materials," *Journal of Applied Physics* **93** (5), 2789-2796 (2003).
- [21]. A Verma, TC Goel, RG Mendiratta, and MI Alam, "Dielectric properties of NiZn ferrites prepared by the citrate precursor method," *Materials Science and Engineering: B* **60** (2), 156-162 (1999).
- [22]. Adel Maher Wahba and Mohamed Bakr Mohamed, "Structural, magnetic, and dielectric properties of nanocrystalline Cr-substituted Co_{0.8}Ni_{0.2}Fe₂O₄ ferrite," *Ceramics International* **40** (4), 6127-6135 (2014).
- [23]. Lijun Jia, Jun Luo, Huaiwu Zhang, Gang Xue, and Yulan Jing, "High-frequency properties of Si-doped Z-type hexaferrites," *Journal of Alloys and Compounds* **489** (1), 162-166 (2010).
- [24]. Muhammad Ajmal, MU Islam, and Absar Ali, "Structural, Electrical and Dielectric Properties of Hexa-ferrite-Polyaniline Nano-composites," *Journal of Superconductivity and Novel Magnetism*, 1-8 (2017). <https://link.springer.com/article/10.1007/s10948-017-4332-x>
- [25]. ON Ivanov and Ya V Trusova, "Electrical conductivity peculiarities of SrTiO₃ZrO₂–ceramic system," *Ceramics International* **42** (4), 5245-5249 (2016).
- [26]. Sujata Sanghi and Ashish Agarwal, "Rietveld refinement, electrical properties and magnetic characteristics of Ca–Sr substituted barium hexaferrites," *Journal of Alloys and Compounds* **513**, 436-444 (2012).